Influences of Local Sea-Surface Temperatures and Large-scale Dynamics on Monthly Precipitation Inferred from Two 10-year GCM-Simulations

Y. C. Sud, G. K. Walker [+], Y. Zhou*, & W. K.-M. Lau

Laboratory for Atmospheres
NASA Goddard Space Flight Center,
Greenbelt, Maryland

POPULAR SUMMARY

It is common knowledge that large-scale, even remote, sea surface temperatures (SSTs) affect major circulation systems such as hurricanes, whereas the local SSTs are pivotal to their intensification or weakening. Indeed, the same principles of physics apply to SST-rainfall relationships on monthly to seasonal as well as interannual time-scales. However, distinguishing among remote and local SST influences remains a challenging problem. Scores of scientists have dealt with the problem by categorizing data and/or analyzing specific situations but without a general methodology for distinguishing among them analytically. By running 2-10 year atmospheric model integrations with two different SST-datasets with a General Circulation Model (GCM), we simulated enough data to attack the problem from "first principles". In sorting the data by SST bins, we discovered: i) evaporation, vertical velocity, and precipitation were very robust and remarkably similar for both simulations; ii) the evaporation increased almost linearly with SST up to about 27^0C where after it leveled off, while the precipitation did not; iii) for almost all SST bins, precipitation correlated much better with the vertical velocity suggesting the influential role of dynamical circulation in addition to SSTs.

Mathematically, the analysis of influence of small perturbations to forcing fields on an output field is well developed. With modern computers, one could use as many fields as physically conceivable and let the perturbation analysis sort out the important ones among them for the problem on hand; however, such an exercise will be prohibitively complex. Alternatively, one can use physical intuition to identify the most important forcing field(s). Since SSTs influence surface evaporation and near-surface moisture transport, we investigated the SST-rainfall relationship through these two fields. Accordingly, the simulated precipitation was

binned by SST and boundary-layer moisture supply. The sorted data helped us compute precipitation change due to i) evaporation increase caused by increase in local SST, but with same external moisture supply, and ii) external moisture supply increase caused by same increase in local SST, but with the same evaporation. The sum of the two gives a quantitative measure of the influence of local SST on the local precipitation everywhere as well as helps to calculate the influence of seasonal variations in SST on the seasonal variations in local rainfall. Several remote and local SST influences were distinguished to better understand the influence of local SSTs on local rainfall vis-à-vis the total simulated rainfall. We found that a double ITCZ of the spring season was caused by remote forcing. The local SST support was paramount for many other tropical rainfall anomalies. Our analysis holds the key to understanding the cause of rainfall anomalies through local and/or remote SST-forcings.

Influences of Local Sea-Surface Temperatures and Large-scale Dynamics on Monthly Precipitation Inferred from Two 10-year GCM-Simulations

Y. C. Sud, G. K. Walker [+], Y. Zhou*,
&
W. K.-M. Lau

Laboratory for Atmospheres
NASA Goddard Space Flight Center,
Greenbelt, Maryland

ABSTRACT

Two parallel sets of 10-year long: January 1, 1982 to December 31, 1991, simulations were made with the finite volume General Circulation Model (fvGCM) in which the model integrations were forced with prescribed sea-surface temperature fields (SSTs) available as two separate SST-datasets. One dataset contained naturally varying monthly SSTs for the chosen period, and the other had the 12-monthly mean SSTs for the same period. Plots of evaporation, precipitation, and atmosphere-column moisture convergence, binned by 1^0C SST intervals show that except for the tropics, the precipitation is more strongly constrained by large-scale dynamics as opposed to local SST. Binning data by SST naturally provided an ensemble average of data contributed from disparate locations with same SST; such averages could be expected to mitigate all location related influences. However, the plots revealed: i) evaporation, vertical velocity, and precipitation are very robust and remarkably similar for each of the two simulations and even for the data from 1987-ENSO-year simulation; ii) while the evaporation increased monotonically with SST up to about 27^0C, the precipitation did not; iii) precipitation correlated much better with the column vertical velocity as opposed to SST suggesting that the influence of dynamical circulation including non-local SSTs is stronger than local-SSTs.

The precipitation fields were doubly binned with respect to SST and boundary-layer mass and/or moisture convergence. The analysis discerned the rate of change of precipitation with local SST as a sum of partial derivative of precipitation with local SST plus partial derivative of precipitation with boundary-layer moisture convergence multiplied by the rate of change of boundary-layer moisture convergence with SST (see Eqn. 3 of Section 4.5). This analysis is mathematically rigorous as well as provides a quantitative measure of the influence of local SST on the local precipitation. The results were recast to examine the dependence of local rainfall on local SSTs; it was discernible only in the tropics. Our methodology can be used for computing relationship between any forcing function and its effect(s) on a chosen field.

1. INTRODUCTION

It is common knowledge that during the warm and cold phases of El Nino Southern Oscillation (ENSO), the intensely raining regions of tropical oceans follow the warm SSTs (Giannini et al., 2001). This is reasonably simulated by most of the modern General Circulation Models (GCMs; Latif et al., 2001). One naturally finds scores of articles employing observations as well as model simulations which show that local SST anomalies are the primary driver of many observed precipitation anomalies particularly in the tropics (e.g., Chen 2005, Hui et at., 2001, and several others). However, we also know that ENSO induced changes in tropical circulation vitally influence both weather and climate in several mid- and high- latitude regions, where SSTs did not change. Evidently therefore, the tropical SST-anomalies have the ability to influence distant regions through dynamics. It can be argued pedagogically that both *in situ* SSTs and dynamic influences are important for precipitation; therefore, discerning among their contributions is vital for understanding the relationship of observed precipitation anomalies in response to large-scale SST anomalies, the primary drivers of observed weather and climate variations in many parts of the world. However, because the dynamics and local SST-influences interact with each other, any modulation of one would affect the other as well as the overall outcome. Therefore, for a broad-view, the influence of only small SST-perturbations that do not alter the large-scale circulation substantially is plausible; otherwise, the only option is a full blown GCM simulation.

The posed question has been variously addressed for some targeted regions both for atmospheric and oceanic circulation regimes (e.g., Lin et al., 2006, Lohmann et al., 2002, Harrison and Craig, 1993; Yu et al., 1991; Bony et al, 1997; Lau et al., 1997). There are parallel examples for land rainfall wherein the influence of soil moisture on rainfall is investigated (e.g.,

Koster et al., 2004). In the Koster et al. multi-model data analysis, different models produced such widely different outcomes that the importance of a model's ability to represent the influence realistically was noted, but it remained an unresolved issue. Indeed, even for our investigation, the SST-evaporation-rainfall interaction may be GCM-dependant. However, first and foremost, we need a robust methodology for delineating the competitive roles of local-SST and all non-local SSTs with feedback processes influencing the circulation dynamics (hereafter dynamic influences) that affect near-surface moisture convergence and precipitation. Nevertheless, both local SST and dynamics are often intertwined and without a mathematically rigorous methodology, the SST-rainfall relation might not be satisfactorily addressed. Lin et al. (2006) analyzed the increase of precipitation efficiency and boundary layer moisture transport toward upper troposphere as a function of SST in tropical deep-convective systems. The work illustrated the need to include the dynamically induced boundary layer moisture convergence as a key component of the SST-rainfall relationship.

The 4-Dimensional Data Assimilation (4DDA) data are commonly called "the best estimate of observations". These data can be very useful for the analysis of issues such as SST-rainfall relationship except that the 4DDA process infuses a discernible degree of pollution into some of the key fields such as vertical velocity and precipitation, which renders the data unfit for a credible scientific research. Moreover, all data assimilation processes have intrinsic mismatches between observed and simulated data; it is partly due to biases of the assimilation-system, the centerpiece of which is a GCM and partly due to mismatches of scales of observations and grid mean values of the 4DDA system. In comparison, GCM-simulations are valuable internally consistent data sources and allow controlled simulations as well as save the key diagnostic critical to the analysis of the issues. But, if the chosen GCM has large biases, the GCM-based inferences merely contribute to uncertainty as opposed to useful solutions of the problem(s), e.g.,

in Koster et al. (2004) study, the authors simply averaged all model outputs for the best answer. Since, precipitation is one outcome of complex interactions among SSTs, large-scale dynamics, and a host of physical processes some of which are not well represented in models, GCM results are often viewed as a model dependant calculation. Therefore one faces the proverbial dilemma--how to discern between the model-characteristics and the true behavior of the atmosphere. Nevertheless, we advocate, if 4DDA fields and observations are used as a guide, simulated data can be very helpful for addressing such problems. Hence we chose the model simulation route and use a well validated GCM with the hope of validating our results with other GCMs.

The finite volume GCM (hereafter fvGCM) is the model of our choice. It is a GSFC model with fv-hydrodynamics and several features of NCAR surface fluxes and NASA/GSFC physics, is described in Section 2. Even though it is one of the best, it shows some biases in the strength of the ITCZ and/or some regional precipitation patterns; however, the simulated precipitation fields in the 10-year mean (Fig. 1a) and observations (Fig. 1b) agree reasonably. Its seasonal cycle (not shown) also has several remarkable similarities with observations. This motivated us to examine the SST-precipitation relationship using its simulations. Regardless, a GCM based inferences are only as good as the GCM simulating them. However, we can expect our results to serve as background for the simulated precipitation analysis in selected regions, such as evidenced in Bony et al. (1997) and Lin et al. (2006) research.

2. MODEL DESCRIPTION

The fv-NCAR GCM used in this research has a finite-volume dynamical core that was developed and extensively evaluated by Lin and Rood (1996) and comprehensively documented by Lin (2004). Except for the radiation and cloud schemes, the model-physics (including the Community Land Model version 2.0 – CLM2) are from the NCAR CCM3.6 community model

(Hurrell et al., 1998). Microphysics of clouds with Relaxed Arakawa-Schubert Scheme (McRAS) is the cloud physics employed in this fv-NCAR GCM version. McRAS was developed at GSFC and was variously found superior to other potential choices (Maloney and Hartman, 2002; Maloney, 2003; Sud et al., 2005). McRAS is structured around the moist convective core of the Relaxed Arakawa-Schubert Scheme (RAS) developed by Moorthi and Suarez (1992) together with Sundqvist (1988) and Tiedtke (1993) cloud microphysics. Its evaluations and upgrades are described in four key papers {Sud and Walker 1999a, b, 2003, 2004}. McRAS tracks cloud amounts through a prognostic cloud mass and cloud water substance equation in which cloud and precipitation microphysics remain fully interactive at all times for all simulated clouds and for cloud types.

The radiation physics schemes (Chou and Suarez, 1994) were also developed and extensively tested at GSFC. Several radiation-transfer algorithms were upgraded and extensively discussed in Chou et al. (1998) & Chou et al. (1999). The scheme performs radiative transfer calculations using cloud water, water vapor, and temperature fields simulated and/or modified by McRAS. These schemes have replaced the cloud and radiation schemes of the fv-NCAR GCM and our new version may be called fv-McRAS GCM (hereafter, simply fvGCM). This model was assessed vis-à-vis the original fv-NCAR GCM by Sud et al. (2005) for influence of SSTs on rainfall and found superior to the original fv-NCAR GCM. The model resolution is 1.0 x 1.25 degrees latitude by longitude, with 55 vertical levels covering the atmosphere from the ground surface to an altitude of approximately 75 km.

3. DATA & SIMULATIONS

All numerical simulations were made with the fvGCM described in Section 2 and forced with monthly prescribed SST and sea-ice boundary conditions available as monthly data. The

initial conditions for the simulation are taken from a 47-year "spin-up" of the standard fv-NCAR GCM with several months of daily soil moisture updates using observed circulation data. This procedure has its usual drawbacks of not providing observations quality analysis, but it is a better alternative to performing extensive soil moisture analysis with a crude land-hydrology model of another data assimilating model using *in situ* observations that in likelihood are likely to be inconsistent with the GCM's resolution. We made two integrations spanning the 10-year simulation period, January 1, 1982 through December 31, 1991. The first integration was forced with the naturally varying monthly SSTs taken from Jones et al. (2001) analysis, and the second was forced with mean monthly SST generated for the 10-year period defined above. All SSTs were prescribed as monthly data, and linearly interpolated to yield the daily SSTs estimates needed by the fvGCM. Besides SSTs, the biosphere, with its phenology and morphology, was also prescribed. In the upper atmosphere, the ozone was climatological and prescribed as monthly data. Everything else, e.g., clouds, cloud-radiation interaction, land hydrology in association with soil moisture, as well as the simulated circulation are fully prognostic and interactive. Thus fvGCM simulations, with additional diagnostics of PBL-moisture convergence and vertical velocity at sigma levels can help us delineate the local SST versus dynamic effects within a model-environment in which all other biogeophysical feedback interactions are simulated by the model's physics and dynamics.

4. RESULTS

We have used both sets of simulations described above to infer the local versus non-local SST influences on the simulated monthly precipitation using the monthly mean fields and using a mathematically rigorous methodology outlined in Sections 4.4 and 4.5.

4.1 SST- Precipitation Fields

In the 10-year averages shown as 2-D plots, the SST distributions are shown through background colored patterns, whereas the precipitation distribution is contoured--both for observations (Fig. 1a) and fv-McRAS GCM simulations with analyzed SSTs (or Cs; Figs. 1b). The isopleths of SST are not parallel to isopleths of precipitation except in the tropics. The intersection angle between them varies from place to place. This essentially suggests that SST-precipitation fields do not correlate well outside of tropics. However, even ocean evaporation can also be complex. It is forced by SST as well as affected by other geophysical fields, such as winds, humidity, and removal of water vapor by the moist processes such as moist convection and PBL growth. Moreover, the annual cycle of evaporation (with interannual SST variability) and associated changes in circulation makes the outcome quite complex; however, in the second parallel set of simulations in which the SST was devoid of interannual variations, a number of inferences were self-evident, which indicate that SSTs affect precipitation distribution either through local effect or by its influence on large-scale dynamics/circulation patterns. Hence we probe into different aspects of the SST-precipitation relationship more critically.

4.2. Precipitation, Vertical Velocity, and Evaporation Binned by SST

The 10-year simulated monthly data for evaporation, precipitation, and vertical velocity were binned by 1^0C SST intervals and plotted. Figure 2 shows each of the four fields with superposed standard deviation (displayed as grey background) for the interannually varying SST simulation (or Cs). Similar means and standard deviation were produced for climatological SST-simulations (or Cc) as well as for a single ENSO year, 1987 (or Ce). However, for clarity only the mean fields (without the standard deviation) are superposed on the Cs fields. This conveys the picture quite well because the standard deviations of Cc and Ce simulation were very similar to Cs. We

also see that the bin-averaged values of Cc and Ce simulations are also very similar to Cs except for high-end SSTs, i.e., SSTs greater than 29°C, where the standard deviation is very large and influence of local SSTs dominate (as we shall see). This clearly suggests that binning captures the essence of the SST-influence for each of the key fields (Figs. 2a-d).

We note that only the bin-averaged monthly evaporation increases monotonically with SST (not exponentially as may be expected from Clausius-Clapeyron relation between saturation humidity and temperature) up to about 26^0C and then it levels off (Fig. 2a); in fact, it reduces slightly at SSTs close to 30^0C. This happens in intensely raining regions. Regions of reduced evaporation appear in strongly converging humid regions, such as the warm pool. In these regions, the wind-speed decreases while the near surface humidity remains high and that is a prime cause of lower evaporation (Chou et al., 2005). We also know that convective downdrafts and sudden wind bursts help to promote local evaporation and presumably that is how the surface evaporation gets some of its boost to maintain the level of local evaporation of the comparatively cooler regions. Alternatively, since moist convection is the primary sink of boundary-layer moisture; its by-product, i.e., precipitation, generates condensation heating that counters the regional radiative cooling. According to Larson and Hartmann (2003) analysis, cooling by radiation is the primary determinant of convective condensation and rising motion over tropical oceans; evaporation merely balance the energy budget at the surface and fulfills the water vapor deficit between moisture consumption by moist convection and moisture convergence that transports moisture into the region. Even the standard deviation of evaporation is quite similar all through except for the warmer SST bins, where intense convective activity generates transients and large temporal variability. Thus large standard deviation of all four quantities at around 30^0C is an outcome of variations due to episodic behavior of the dynamics of deep convection as well as reduced bin-population (smaller by a factor of 50-100). Moreover, some geographic

location may have persistent warm SST and low precipitation. This suggests that intensity of episodic convection increases with SST while the mean does not change much (elaborated further in Section 4.3). On the other hand, the relationship between SST and precipitation is much more constrained by dynamics. The bin-averaged precipitation has four regimes. In the high latitude regime comprising of SST range of 0-9^{0}C, the precipitation increases with SST; in the second mid-latitude regime comprising of SST range of 9-24^{0}C, the precipitation decreases with SST. Thereafter, in the tropical regime comprising of SST range of 26-29^{0}C, the precipitation increases very quickly with the SST. Finally, for SST warmer than 29^{0}C, the precipitation starts to decrease again. These patterns have a good correlation with the bin-averaged vertical velocity (Fig. 2c). Since the mid-latitudes supply moisture to the tropics through the Hadley circulation and to the high latitudes through Farrel circulation, the precipitation in mid-latitudes is less than the evaporation. The precipitation reduction is far larger on the tropical side of mid-latitudes as compared to the baroclinically dominated high-latitudes. Consequently, the behavior of the precipitation in the binned SST plots is an outcome of rate of moisture transport out of mid-latitudes. Hadley circulation of the tropics, associated with relatively smaller Coriolis force, but with abundance of moisture, produces significantly large condensation heating. Accordingly, Hadley circulation is much stronger (than the Ferrell circulation) and is accompanied by larger circulating air masses and associated moisture convergence(s). In short, the moisture loss and associated precipitation reduction on the tropical side of mid-latitudes leads to large precipitation reduction in the regions of increasing SST and evaporation, *a finding counter to popular axioms like precipitation increases with SST.* . However, there is much better correlation between the tropospheric-mean (800-300hPa) vertical velocity and precipitation (Figs 2b & c), both of which are dynamics-controlled and SST-forced. Such a correlation gives the appearance of a large vertical velocity precipitation relationship.

However, it is an outcome of the much stronger ability of tropics to utilize diabatic heating caused by large condensation to force near surface mass convergence that brings warm moisture-laden air carrying mid-latitude evaporation (Fig. 2d). In fact, it is the joint influence of large-scale dynamical organization of circulation systems in response to large-scale structures of SSTs that are so ubiquitous in the tropics. These structures manifest through negative correlation between SST and vertical velocity and precipitation in the medium-SST mid-latitude regions. The outcome is robust while dynamic constraints convolve to exacerbate the SST forcing; but any conclusion about the influence of SST on vertical velocity and the associated precipitation has its pitfalls unless it is viewed in the light of the dynamical response of the circulation. This is discussed in Bony et al. (1997). Indeed, there is large variability in the standard deviation of each of the fields; while a large reduction in all of them near the highest SSTs represent regions that lack alignment of atmospheric convection with SSTs because it is modulated more by atmospheric dynamics and not by oceanic circulation with its radiative forcing that generates hot spots. The emergence of hot spots in the sinking tropical regions was noted by Waliser's (1996) who suggested that solar heating in non-precipitating clear regions is its primary cause; however, in the prescribed SST simulations, cloudiness-SST feedbacks do not exist and we still find reduction of average rainfall with SST larger than 30^0C. Such an outcome is a consequence of the inability of some warm regions to better align with the circulation systems of the region due to their geophysical juxtaposition enabling precipitation to be out of phase with warm SST in certain area and some times. In other words, even though there are warm regions, they are unable to capture as much convergence and precipitation as others region with smaller SST because they are not well aligned with large organized tropical systems that benefit from significant large-scale moisture convergence. Large tropical convergence not only promotes deep convection but also dries and cools the near surface region by downdrafts (Sud and Walker, 1993), an essential player

that has been inadequately parameterized in the cloud physics of GCMs up until recently. Why then does the influence of non-alignment emerge at high temperatures? It is because at the higher end of SSTs, the grid cells involved are much fewer and their collective ability to affect the atmospheric circulation is accordingly reduced. In other words, the alignment of atmospheric circulation to SSTs is based on large-scale SST fields wherein the total number of grid cells involved also count for the outcome.

One also notes that a strong SST precipitation relationship starts to emerge above 27^0C where the bin-averaged sinking motion (seen at lower SSTs), suddenly changes into the bin-averaged rising motion. This enables upward transport of moisture and that triggers moist-processes which consume moisture provided by local evaporation and moisture convergence. Thus, above 27^0C SST, the precipitation begins to exceed evaporation. This is roughly the temperature at which deep convection ensues. Its characteristic behavior has been exhaustively discussed by Sud et al. (1999) using TOGA-COARE data and applying fundamental principles of moist convections enunciated by Arakawa-Schubert (1974) and used in RAS -- the backbone of moist convective physics of McRAS. However, there are some discernible biases in the moist convective parameterizations of our times and those naturally warrant some caution even though our analysis is principally rigorous (see Section 5). The SST-binned PBL moisture convergence closely corresponds with vertical velocity, particularly in the tropics: SST between 26°C and 29°C, this represents large-scale convergence associated with ITCZ/SPCZ; it is only partly due to the increase of PBL moisture content as suggested by Lin et al.(2006) for deep convective systems of tropics.

4.3 Global Evaporation and Column Moisture Convergence

The primary moisture sources for precipitation are surface evaporation (Fig 3a) and tropospheric moisture flux convergence: $-\int_{ps}^{pt} \nabla_p . V_p q \, dp$ (Fig 3b). Here V_p is the horizontal velocity, q is water vapor mixing ratio and $\nabla_p . \psi$ is the horizontal divergence of a vector field, $\psi = V_p q$. We can subdivide the column moisture convergence into two parts, one associated with the mass flux convergence: $-\int_{ps}^{pt} q \nabla_p . V_p \, dp$, so called first term (Fig 3c), and one associated with humidity gradient: $-\int_{ps}^{pt} V_p . \nabla_p q \, dp$, so called second term (Fig 3d). We note that the similarity of patterns between the total moisture convergence and the first term is quite remarkable; it shows moisture carried by mass convergence is a primary contributor of total moisture convergence. It also explains the relationship between binned precipitation and vertical velocity discussed in Section 4.2 and delineated by Bony et al. (1997). The second term is negative over most oceanic areas. It shows that the entire humidity gradient fields of the tropical and exptratropical oceans work as moisture source for a few intensely precipitating regions such as the ITCZ, the SPCZ, and the warm pool. The only exception is the cold-tongue region of the Equatorial Western Pacific as well as small precipitating regions at high latitudes. The negative correlation between SST and precipitation, in 9-24^{0}C SSTs range, is closely associated with sinking region of mid-latitudes. The reduced precipitation at SST warmer than 29^{0}C is also associated with reduced rising motion. However, they were adequately discussed in Section 4.2.

4.4 Evaporation, Moisture Convergence in the PBL, and Precipitation

A general understanding of the role of SSTs and near surface (PBL) and upper level moisture flux convergence can be addressed by a standard differential equation of n-variables of which we use only three:

$$d\zeta = \frac{\partial \zeta}{\partial T_{ss}} \delta T_{ss} + \frac{\partial \zeta}{\partial M_b} \delta M_b + \frac{\partial \zeta}{\partial M_t} M_t + \ldots, \qquad (1)$$

where T_{ss} and M_b & M_t are SST and associated moisture flux convergences in the boundary layer and aloft that primarily modulate a scalar ζ. Such an analysis can be useful if the other effects are either small or cancel out in the bin-averaged data. The ζ field could be any diagnostic quantity such as precipitation or cloudiness. Assuming that evaporation, SSTs, and PBL mass and moisture flux divergences are the primary determinant of precipitation, the analysis can reveal the relative roles of small changes in local and non-local SSTs and resultant moisture convergence changes. We claim that SST, through surface fluxes, and PBL mass/moisture convergence are two dominant forcing functions that affect precipitation. In doubly binned analysis, Fig. 4, evaporation, PBL moisture convergence and precipitation are binned by equal intervals of SST and PBL-mass divergence. A 2^0C SST-bin interval mitigates the influence of small change in SSTs due to daily varying SSTs whose non-linear effect could not be taken onto account. Clearly, $d\zeta \equiv 0$ defines isopleths of ζ. Vertically (horizontally) oriented isopleths show lesser (larger) dependence on near-surface mass divergence and hence the vertical velocity. Moreover, lesser dependence on mass divergence may imply larger dependence on SSTs since we know that both mass/moisture convergence and evaporation are affected by SST. In addition, large gradients among the isopleths imply stronger dependence.

We now probe into the individual fields to get a little better insight. As shown in Section 4.3, the PBL moisture flux convergence: $-\int_{ps}^{800} \nabla_p . V_p q \, dp$, too can be divided into two terms. The first term gives mass convergence dependant moisture convergence: $-\int_{ps}^{800} q \nabla_p . V_p \, dp$, while the second term gives humidity gradient dependant moisture convergence: $-\int_{ps}^{800} V_p . \nabla_p q \, dp$. The plots for the thusly partitioned terms are not shown (see Section 4.3), but moisture convergence as such helps to relate the near surface evaporation and moisture convergences as functions of SST and PBL mass convergences that primarily influence the moisture supply to the cloud base for moist convection.

The new analysis provides a lot of valuable insight. Surface evaporation increases with SST as should be expected (Fig. 4a); however, the isopleths of evaporation requires higher SSTs at/near zero convergence, particularly for SSTs colder than 15^0C. These SSTs are associated with the baroclinic activity in the atmosphere aloft; strong convergence or divergence is often associated with synoptic scale circulation systems that influences PBL mass convergence (divergence) into a low (or a high) pressure system. Since regions of larger mass convergence are associated with stronger wind speeds that promote evaporation, larger convergence or divergence would be able to maintain the same evaporation at lower SSTs, which explains the peculiar shape of the isopleths. The pattern breaks down for warmer SSTs because there is more quasi-stationary flow at those latitudes. Between 18-24^0C, the mid-latitude subsidence regions are major suppliers of moisture to the ITCZ/SPCZ regions with precipitation using local surface evaporation and water vapor transported as horizontal moisture flux. The maximum evaporation occurs at

some moderate divergence (~0.005 Kg m^{-2} s^{-1}). The regions of high convergence and less evaporation as well as precipitation (Fig. 4c) are mostly coastal regions in the SST range of 15-22^{0}C with mass convergence of 0.01 to 0.02 Kg m^{-2} s^{-1}}. Some of them are off the west coast of North and South America where high vertical velocities are generated by orographic features of the Andes without much precipitation. In large-convergence high-SST regions, there is larger evaporation as well as precipitation. These are the well known ITCZ and warm pool regions. Overall, in almost all converging (diverging) regions, precipitation is larger (smaller) than evaporation. However, the dependence of precipitation on SST and mass convergence can be inferred from the gradients of isopleths. The ITCZ is found in strongly converging regions of SSTs > 28^{0}C. The strongest convergence is in the western tropical pacific where the dependence on SSTs is quite strong; whereas the influence of mass convergence is less, as inferred from the vertical orientation of the precipitation isopleths. The tongue of larger precipitation between 18-24^{0}C and around 0.003 to 0.006 Kg m^{-2} s^{-1} convergence is largely associated with mid latitude (~30N and ~30S) storm tracks.

The associated PBL moisture convergence (Fig. 4b), which again correlates to mass convergence related moisture convergence (not shown), is evidenced in the correlation; it is positive (negative) in converging (diverging) regions. In the ITCZ regions, both PBL moisture convergence and surface evaporation are much larger than the precipitation. Such differences can be viewed as precipitation efficiency. In the coastal areas, it is very low. In other areas, it gets very close to 100% because moisture is also being supplied by moisture flux-transports above the boundary layer. In binning precipitation by 1^{0}C for tropical regions, one sees more details (not shown, because such a fine resolution is unsuitable for the analysis in Section 4.5). It shows reduced

precipitation above 30^0C, the so called non-aligned warm regions that hang in without much convergence or evaporation.

4.5 Splitting Precipitation by SST and PBL Moisture Convergence

We extend the analysis defined by Eq. (1) to compute partial derivatives of key determinants of precipitation in order to better analyze the behavior of precipitation in response to local SST and then obtain the dynamic influence that include all other effects including that of non-local SSTs as a residue. We rewrite (1) to apply it to precipitation in each bin and use the first two terms as follows:

$$dP = \frac{\partial P}{\partial T_{ss}}\delta T_{ss} + \frac{\partial P}{\partial Mc}\delta Mc . \qquad (2)$$

For total derivative of P with T_{ss}, Eq. (2) is recast as:

$$\frac{dP}{dT_{ss}} = \frac{\partial P}{\partial T_{ss}} + \frac{\partial P}{\partial Mc}\frac{dMc}{dT_{ss}} . \qquad (3)$$

Here P is precipitation, and MC is PBL moisture convergence in Kg m^{-2} d^{-1}. Evidently, the upper level convergence (term 3 of Eq.1) is dropped as secondary to the influence of SSTs on local precipitation. Clearly, the effect of SST is through evaporation; it is implicit in the first term whereas the second term includes the local SST effect in affecting the dynamic moisture convergence. The partial derivatives are determined for the mean values of the data in each bin separated by 2^0C SST and 1 Kg m^{-2} day^{-1} moisture convergence. The assumption being that these bins contain data of similarly forced grid points because the moisture convergences and SSTs are similar for the entire population except for the variability associated with the bin-size. To solve Eq. (3), we calculated the partial derivatives of the bin-mean fields in the horizontal and vertical directions to obtain

the two partial derivatives (Fig. 5a). To obtain the best estimates of dMc/dT_{ss}, the least square regression was attempted first because it had the potential to yield best estimates of dMc/dT_{ss}. However, this calculation failed to provide reasonable derivatives. Indeed, when we examined the sample data, we were unable to see any trend; this is partly caused by daily interpolated SSTs and is compounded by data obtained from disparate places; however, average dMc/dT_{ss} could be estimated from BL-Mc binned by SSTs (Fig. 2d). The two terms of Eq. (3) are shown in Fig. 5a. where the rate of change of precipitation is plotted as a function of SST and PBL moisture convergence.

Typically, $\partial P/\partial T_{ss}$ can be expected to be positive, but sometimes it can become negative when higher SST warms the PBL and helps to mix the evaporating, even converging, moisture into drier sinking and diverging air aloft; under such conditions, vertical mixing helps the moisture to escape (classical Sahara desert scenario where near surface moisture convergence escapes by mixing into the dry diverging air aloft, Sud and Molod, 1988), however, $\partial P/\partial Mc$ is almost always positive while dMc/dT_{ss} is strongly positive in tropics and discernibly negative in regions of subtropical high.

The focal relationship is between rates of change of SST versus rate of change of precipitation, dP/dTss. It is large in the tropics (SSTs between 25-30^{0}C). Here local SST-induced evaporation and near surface moisture convergence work in concert to increase the precipitation and that is a well known tropical phenomena which lead Bony et al. (1997) and Lin et al (2006) to search the tropics for SST-rainfall relationship. Interestingly, its dependence on PBL moisture convergence is not so critical for the overall outcome because the calculation is for obtaining the influence of SST on increased Mc as opposed to the other way around; however, the outcome is also evident

in the verticality of isopleths. The response of precipitation to increasing SST in the tropics is up to 1.5 mm d^{-1} C^{-1}. On the other hand, in the diverging region of high SST, both partial derivatives are small while dMc/dTss is negative; so the sum of the two can be slightly negative. In other words, small increase in SST can lead to reduction in precipitation, a picture that is consistent with Fig. 2b. The values range from 0.5-1.00 mm/day for SSTs and 0-0.4 mm/day for moisture convergence. This circulation is consistent with warm regions transporting moisture into the ITCZ or SPCZ regions. Nevertheless, how-so-ever small, there is a positive contribution of both SST and moisture convergence except for highly subsiding regions. Some areas of small negative $dP/dT_{ss} < 0$ imply that the increase in evaporation is mitigated by increased upward mixing of moisture that subsequently manages to escape with subsiding and diverging dry air aloft. It represents the drying influence of shallow convection. In low-SST high latitude regions, SSTs are not very important, while boundary layer Mc contributes to majority of the precipitation, but with less than 100% precipitation efficiency. Precipitation yields larger than 100% of Mc imply moisture supply at the upper levels and that was seen in some of the regions (not shown).

Figure 5b shows the projection of dP/dT_{ss} analysis on to the global scale SST-fields. This graphically illustrates how different SST-domains are affected by varying SSTs on monthly time; the data was averaged over the 10-year simulation period. Its standard deviation reflects both inter-annual and intra-annual variability of the monthly rainfall response to local SST. Such a result is useful for global change scenarios and even understanding the influence of sudden perturbations in SST in limited regions due to anthropogenic activity or extra terrestrial impingements.

4.6 Local SST-Rainfall yields in the 10-year Annual Cycle

Figure 6 shows very interesting correspondences between total and local SST produced rainfall changes projected from calculations of Section 4.4 and based on the fvGCM simulations for each of the 4-seasons. The first inference is that many regions of large positive (negative) total rainfall differences correspond well with the local SST caused rainfall changes. In examining JJA differences, Northern tropical latitudes at around 20N produce large increases in total rainfall; this is in unison with increased influence of local SST. The opposite is the case for JJA over Southern Pacific Oceans. The Atlantic ITCZ rainfall increases also happen in concert with local SSTs produced increases in rainfall and vice versa. Nevertheless, over northern Atlantic, where SSTs are warmer (suggesting an increase in rainfall due to local SSTs), actually there is a decreases due to large scale dynamics that enhances moisture divergence over the oceans while MC over North America and Africa increases due to significant increase in thermally induced large-scale flow.

In winter, DJF, the Sun is in the Southern Hemisphere where the landmass is limited, therefore the SSTs dominates the outcome that is reflected through a better correspondence between local SST produced rainfall increases and total rainfall. On the other hand, spring season, MAM, is well known for its double ITCZ in the tropical western Pacific. It happens in both the fvGCM simulations and observations data. Since the SST based local rainfall changes have no such structure, we argue that double ITCZ of the spring season is largely a dynamics phenomenon and the current findings agree with our past analysis of model simulations. Interestingly, fall-season, SON, always has a single ITCZ, while as compared to the spring season, it emerges as a double negative rainfall anomaly (a negative image of MAM) on either side of the ITCZ; this too is largely

dynamic controlled even though it has some SST support because the local SST influence is positive at the ITCZ location and slightly negative on both sides of it. We can interpret it as a small positive contribution of local SSTs. In comparing MAM and SON rainfall anomalies of the tropics, one sees dramatic reversal of anomaly patterns, and those are consistent with warmer (cooler) western tropical Pacific in the MAM (SON) seasons. The differences in rainfall anomalies may also be related to larger (smaller) solar forcing is MAM (SON). Hence, it is reasonable to expect that the dynamic influences must be paramount for the simulated pattern-differences. Overall when ever and where ever rainfall anomaly patterns parallel the SST produced local rainfall change patterns, local SST has some influence, but often it is partial, e.g., over Southern Pacific in DJF or Northern Pacific in JJA on the western side; but when the patterns do not align, the influence has to be largely dynamic, e.g., emergence of double ITCZ in western tropical Pacific in MAM. However, the influence of differential land heating due to solar forcing as a dynamic influence can not be ruled out.

Indeed, the analysis shows that most of the SST influence on rainfall is through large-scaled organization and not as a response to local SSTs, a finding consistent with all the previous diagnostics. The explanation for the emergence of hot spots at high-end of SSTs is also consistent with the notion that grid-scale changes in SST are unable to influence the global circulation.

5. CONCLUSIONS and SUMMARY

Several investigations have explored the influence of SST and remote forcing on the local precipitation, particularly with the goal of understanding the influence of tropical SSTs on precipitation. However, because the local SST and dynamic effects are intertwined, it is difficult

to discern among them without a binning-type of analysis. Some earlier works made concerted efforts to untangle the puzzle for the tropics by binning and categorizing the data by SST and vertical velocity at 500hPa (Bony et al., 1977) and even mass divergence (Lau et al., 1997) while several others relied on physical arguments to resolve the puzzle, but a quantitative assessment of the influence of SST anomalies on rainfall that is mathematically rigorous and would have universal application has not emerged so far. Indeed, two of the coauthors of Bony et al. (1997) were unable to separate these two effects in quantitative way which has now become possible.

If SST changes are large, the only realistic option is to perform simulation experiments; however, for a broad understanding of issues, a binning analysis could serve as a useful guide for the specific modeling and/or observational studies. Binning is a way of averaging out the influence of geographic juxtapositions and grouping data for similarly forced regions. However, in binning by SST-alone, the influences of dynamic forcing does not cancel out even with averaging disparate data drawn from different locations! On the hind side, it is evident why it should not be expected. The coupled Earth-Atmosphere system has a lot of intrinsic internal organization together with large systematic (zonally and temporally stratified) solar forcing. Bony et al. (1997) worked around it by categorizing data by vertical velocity. However, a straight forward SST-binning for simulations with normally varying and climatologically varying SSTs led us to infer that: i) the SST-binned moisture, vertical motion and precipitation fields are very robust; ii) the evaporation increases monotonically with SST up to about 27^0C after which it plateaus, iii) the precipitation correlates more with vertical velocity and not as much with local SST or evaporation; iv) overall, the influence of dynamical circulation is stronger than that of the SST; v) moisture convergence is strongly associated with mass convergence as opposed to humidity gradients (missing in the analysis) that are functions of SST-gradient, vi) the hot spots, defined as small regions of large SSTs but lesser

rainfall comprise of regions that do not align with centers of organized convergence so they also emerge in prescribed SST simulations.

When we examined doubly binned precipitation fields with respect to SST and PBL mass as well as moisture convergence to determine dP/dTss, there was a very worthwhile result. We interpreted the fvGCM-simulated data through a partial differential equation that could be applied to doubly binned precipitation. This delineated rigorously the influences of local SST versus dynamically forced PBL moisture convergence effects. In the context of a ten year global circulation, the precipitation is seen to emerge as a function of local SST given by $\partial P / T_{ss}$, and moisture convergence $\partial P / Mc$, and the influence of SST on changes in moisture convergence, $\partial Mc / T_{ss}$ whose joint effect is captured by Eq. (3). We produced global plots revealing the key roles of SST in influencing the global circulation.

Clearly, even though we have not discovered anything fundamentally different from several earlier pioneering works, the present analysis quantifies the influence of local SST on precipitation in a manner not performed before. The new analysis provides a quantitative solution to the SST rainfall relationship problem. We advocate that our analysis may be more useful for climate change assessment and in deciphering the influence of SSTs on rainfall in different climate regimes. The outcome of the analysis has also been projected on to SSTs globally; it helped us to quantify rainfall changes in response to local SST changes. Its potential advantage can be for more realistic assessments of consequences of SST-changes, e.g., in a global warming scenario, on rainfall in which other binning variables such as cloudiness must be invoked. However, our results also warrant some caution because our data is based on the fvGCM simulation, therefore the findings are limited by the ability of the model to simulate the annual cycle of circulation and rainfall accurately. In the Koster et al. (2004) multi-model analysis of soil moisture rainfall relationship, the major surprise was the wide scatter of predictions even in

well-known models selected for the research; something similar might happen for SST-rainfall relationship! Nevertheless, the proposed methodology with n-variables is mathematically rigorous even though it requires some physical intuition in appropriately choosing the variables influencing the outcome. Overall our results appears reasonable, however, the aforestated caution is our way of informing the readers about the pitfalls. Nevertheless, our analysis provides useful insights for many practical applications while our results remain open to potential upgrades with better model or 4DDA data products.

Acknowledgments. The authors wish to thank Drs. Don Anderson and Tsengdar Lee of NASA HQ for supporting cloud model development research. Participation of Dr. Y. C. Sud and Mr. G. K. Walker is the result of that support. Dr. Yaping Zhou is supported by NASA Earth Science Enterprise's Multidisplinary Research in Climate, Chemistry, and Global Modeling under WBS 509496.02.01.01.07 project.

REFERENCES

Bony, S., K. M. Lau, and Y. Sud, 1997: Sea Surface Temperature and Large Scale Circulation Influences on Tropical Greenhouse Effect and Cloud Radiative Forcing. *J. Climate,* **10**. 2055-2077.

Chen, C., 2005: Relative impact of local and remote SST forcing on the climate predictability. Geophysics Res. Abstracts., **7**, 02869. Euro. Geosc. Union.

Hui S., J. D. Neelin, and C. Chou, 2001: Tropical teleconnection and local response to SST anomalies during the 1997-1998 El Niño. *J. Geophys. Res.*, 106 (D17), 2001.

Chou, M.-D., K.-T. Lee, S.-C. Tsay, and Q. Fu, 1999: Parameterization of cloud longwave scattering for use in atmospheric models. *J. Climate*, **12**(1), 159-169.

Chou, M.-D., and M.J. Suarez, 1994: An efficient thermal infrared radiation parameterization for use in general circulation models. NASA Tech. Memo. 104606, Volume 3, 102 pp.

Chou, M.-D., M.J. Suarez, C.-H. Ho, M.-H. Yan, and K.-T. Lee, 1998: Parameterizations for cloud overlapping and shortwave single scattering properties for use in general circulation and cloud ensemble models. *J. Climate*, **11**(2), 202-214.

Del Genio, A.D., M.S. Yao, W. Kovari, and K.K.W. Lo, 1996: A prognostic cloud water parameterization for global climate models. *J. Climate*, **9**(2), 270-304.

Giannini, A., Chiang, J. C. H., Cane, M. A., Kushnir, Y., Seager, R., 2001: The ENSO Teleconnection to the Tropical Atlantic Ocean: Contributions of the Remote and Local SSTs to Rainfall Variability in the Tropical Americas" Journal of Climate 14: 4530-4544.

Gushchina D., B. Dewitte and S. Illig, 2006: Remote ENSO forcing versus local air-sea interaction in QTCM: a sensitivity study to intraseasonal variability. Advance in Geoscience, 6, 289-297. pdf

Harrison, D. E., and A.P. Craig, 1993: Ocean model studies of the upper ocean variability at at 0°N, 160°W during the 1982-1983 ENSO: Local and Remotely Forced Response. J. Phys. Oceanography, 23, 426-451.

Huffman, G.J., R.F. Adler, P. Arkin, A. Chang, R. Ferraro, A. Gruber, J. Janowiak, A. McNab, B. Rudolf, and U. Schneider: 1997: The Global Precipitation Climatology Project (GPCP) combined precipitation dataset. *Bull. Amer. Meteor. Soc.*, 78(1), 5-20.

Hurrell, J.W., J.J. Hack, B.A. Boville, D.L. Williamson, and J.T. Kiehl, 1998: The dynamical simulation of the NCAR Community Climate Model version 3 (CCM3). *J. Climate*, **11**(6), 1207-1236.

Jones, P.D., T.J. Osborn, K.R. Briffa, C.K. Folland, E.B. Horton, L.V. Alexander, D.E. Parker, and N.A. Rayner, 2001. Adjusting for sampling density in grid box land and ocean surface temperature time series. *Journal of Geophysical Research* 106:3371-3380.

Koster, R. D., P. A. Dirmeyer, Z. Guo, G. Bonan, E. Chan, P. Cox, C. T. Gordon, S. Kanae, E. Kowalczyk, D. Lawrence, P. Liu, C.-H. Lu, S. Malyshev, B. McAvaney, K. Mitchell, D. Mocko, T. Oki, K. Oleson, A. Pitman, Y. C. Sud, et al., 2004: Regions of strong coupling between soil moisture and precipitation. *Science*, **305**(5687), 1138-1140.

Lau, K. M., H. T. Wu, and S. Bony, 1997: The Role of Large Scale Atmospheric Circulation in the Relationship Between Tropical Convection and Sea Surface Temperature. *J. Climate*, **10**, 381-392.

Larson, K. and D. L. Hartmann, Interactions among Cloud, Water Vapor, Radiation and Large-scale Circulation in the Tropical Climate, Part 1: Sensitivity to uniform Sea Surface Temperature changes. *J. Climate*, **16**, 1425-1440, 2003.

Larson, K. and D. L. Hartmann,, Interactions among Cloud, Water Vapor, Radiation and Large-scale Circulation in the Tropical Climate, Part 2: Sensitivity to spatial gradients of Sea Surface Temperature. *J. Climate*, **16**, 1441-1455, 2003.

Latif, M. and Coauthors, 2001: ENSIP: the El Niño simulation intercomparison project, Climate Dynamics, 18, 255-276.

Lehmann, A., A. Krauss, and H.-H. Hinrichsen, 2002, Effects of remote and local atmospheric forcing on circulation and upwelling in the Baltic Sea. Tellus A., 54, 3, 299-361.

Lin, B., B. A. Wielicki, P. Minnis, L. Chambers, K.-M. Xu, Y. Hu, and A. Fan, 2006: The effect of environmental conditions on tropical deep convective systems observed from the TRMM satellite. J. Climat. (accepted).

Lin, S.-J., 2004: A "vertically Lagrangian" finite-volume dynamical core for global models. *Mon. Wea. Rev.*, **132**(10), 2293-2307.

Lin, S.-J., and R.B. Rood, 1996: Multidimensional flux-form semi-Lagrangian transport schemes. *Mon. Wea. Rev.*, **124**(9), 2046-2070.

Maloney, E.D., and D.L. Hartmann, 2001: The sensitivity of intraseasonal variability in the NCAR CCM3 to changes in convective parameterization. *J. Climate*, **14**(9), 2015-2034.

Maloney, E.D., 2002: An intraseasonal oscillation composite lifecycle in the NCAR CCM3.6 with modified convection. *J. Climate*, **15**(9), 964-982.

Moorthi, S., and M.J. Suarez, 1992: Relaxed Arakawa-Schubert: A parameterization of moist convection for general circulation models.. *Mon. Wea. Rev.*, **120**(6), 978-1002.

Sud, Y.C., and A. Molod, 1988: The roles of dry convection, cloud-radiation feedback processes and the influence of recent improvements in the parameterization of convection in the GLA GCM. *Mon. Wea. Rev.*, **116**(11), 2366-2387.

Sud, Y.C., and G.K. Walker, 1993: A rain evaporation and downdraft parameterization to complement a cumulus updraft scheme and its evaluation using GATE data. *Mon. Wea. Rev.*, **121**(11), 3019-3039.

Sud, Y.C., and G.K. Walker, 1999a: Microphysics of clouds with the Relaxed Arakawa-Schubert Scheme (McRAS). Part I: Design and Evaluation with GATE Phase III Data. *J. Atmos. Sci.*, **56**(18), 3196-3220.

Sud, Y.C., and G.K. Walker, 1999b: Microphysics of clouds with the Relaxed Arakawa-Schubert Scheme (McRAS). Part II: Implementation and performance in GEOS II GCM. *J. Atmos. Sci.*, **56**(18), 3221-3240.

Sud, Y.C., and G.K. Walker, 2003: Influence of ice-phase physics of hydrometeors on moist-convection. *Geophys. Res. Let.*, **30**(14), 1758, doi:10.1029/2003GL017587.

Sundqvist, H., E. Berge, and J.E. Kristjänsson, 1989: Condensation and cloud parameterization studies with a mesoscale numerical weather prediction model. *Mon. Wea. Rev.*, **117**(8), 1641-1657.

Tiedtke, M., 1993: Representation of clouds in large-scale models. *Mon. Wea. Rev.*, **121**(11), 3040-3061.

Figure captions:

Figure 1: Composite plots of SST and Precipitation. Shaded areas show the 120-month mean SST in ^{0}C. Contours represent precipitation in mm d^{-1}: GPCP estimates (top panel) and McRAS simulated (bottom panel).

Figure 2: McRAS simulated monthly evaporation (top panel), precipitation (middle panel), and mean upward vertical velocity from surface to 300 hPa (bottom panel), binned by SST. Observed SST simulation data (green line) with standard deviation (shaded) is shown; climatological SST simulation (yellow dashes); and 12-month 1987 El Nino SST simulation (red dashes) are plotted. Units of each field are on the figures.

Figure 3: Latent heat flux and three column moisture convergence terms: (a) latent heat flux, $b) -\int \nabla.Vq$, $c) -\int q\nabla.V$ and $d) -\int V.\nabla q$ for the McRAS simulations. Contour intervals are evident in the figure.

Figure 4: McRAS simulated fields, binned by SST and PBL mass convergence (2C SST bins). Contours show values of a) surface latent heat flux (top), b) PBL moisture convergence (middle), and c) precipitation (bottom). Standard deviation of plotted fields for elements of each bin, except for (c), which shows the standard deviation of PBL mass convergence (kg m^{-2} hr^{-1}).

Figure 5a: McRAS simulated fields, binned by SST and PBL moisture convergence (2C SST; 1 mm d^{-1} moisture convergence). Contours show values of d(P)/d(SST) (mm d^{-1} K^{-1}) within each bin, while the shaded background (range seen in color bar) shows d(P)/d(PBL-MC). Refer to the text for further explanation of this figure.

Figure 5b: Average rate of change of precipitation (mmd^{-1}) for each 1^{0}C rise in local SST projected from analysis in Fig. 5a. Its standard deviation for the analysis period is seen in the color coded background.

Figure 6: Four Panels of seasonal changes in rainfall (mm d^{-1}) in the 10-year simulation divided into: a) influence of local SST (contoured), b) all effects including SSTs and dynamic organization (shaded). Seasons are marked on the panels.

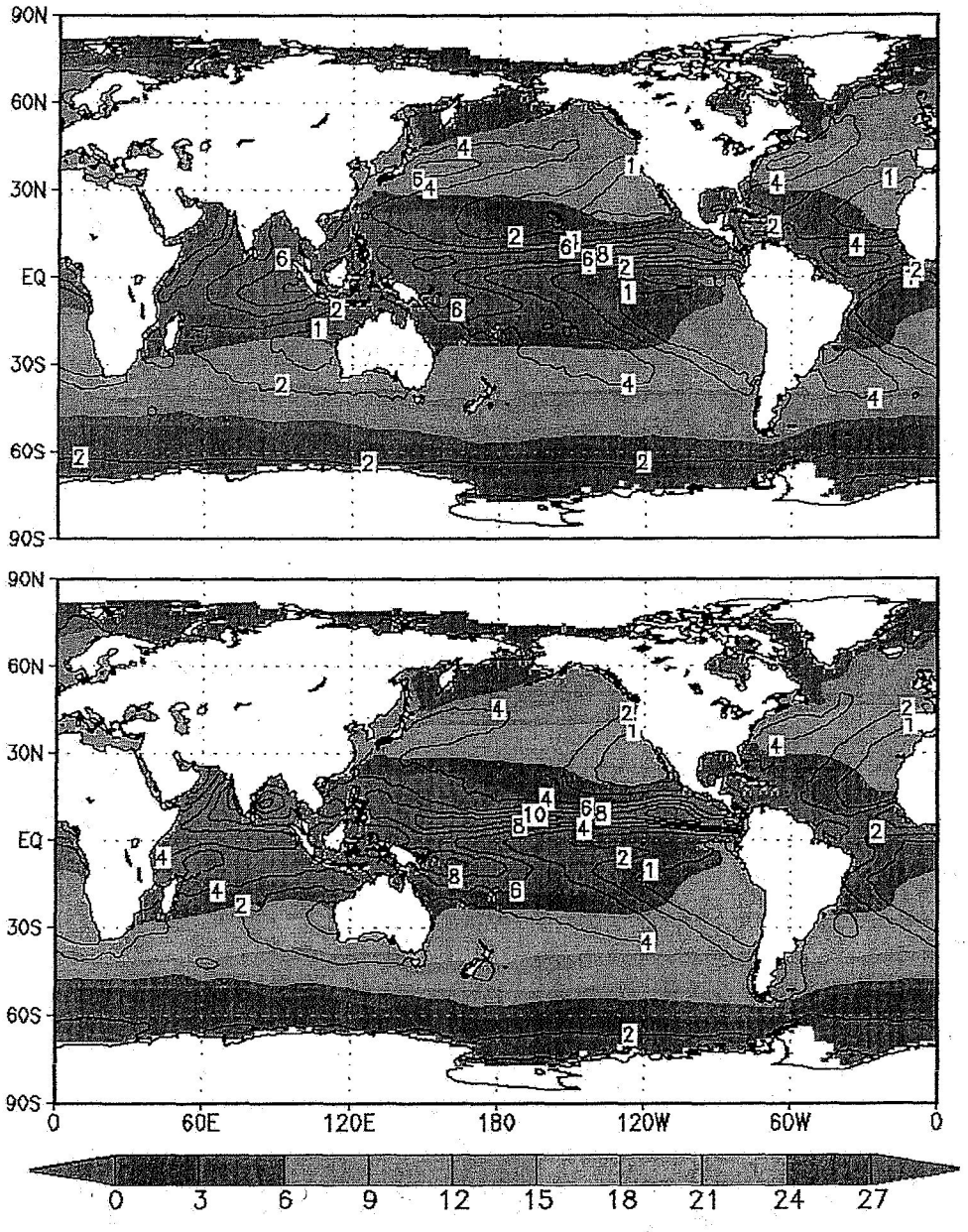

Fig 1. Shaded areas show the mean of the 120-month sea surface temperatures (C) used in the McRAS simulation. Contours represent the GPCP estimated precipitation (mm d^{-1}, top panel) and McRAS simulated precipitation (bottom panel).

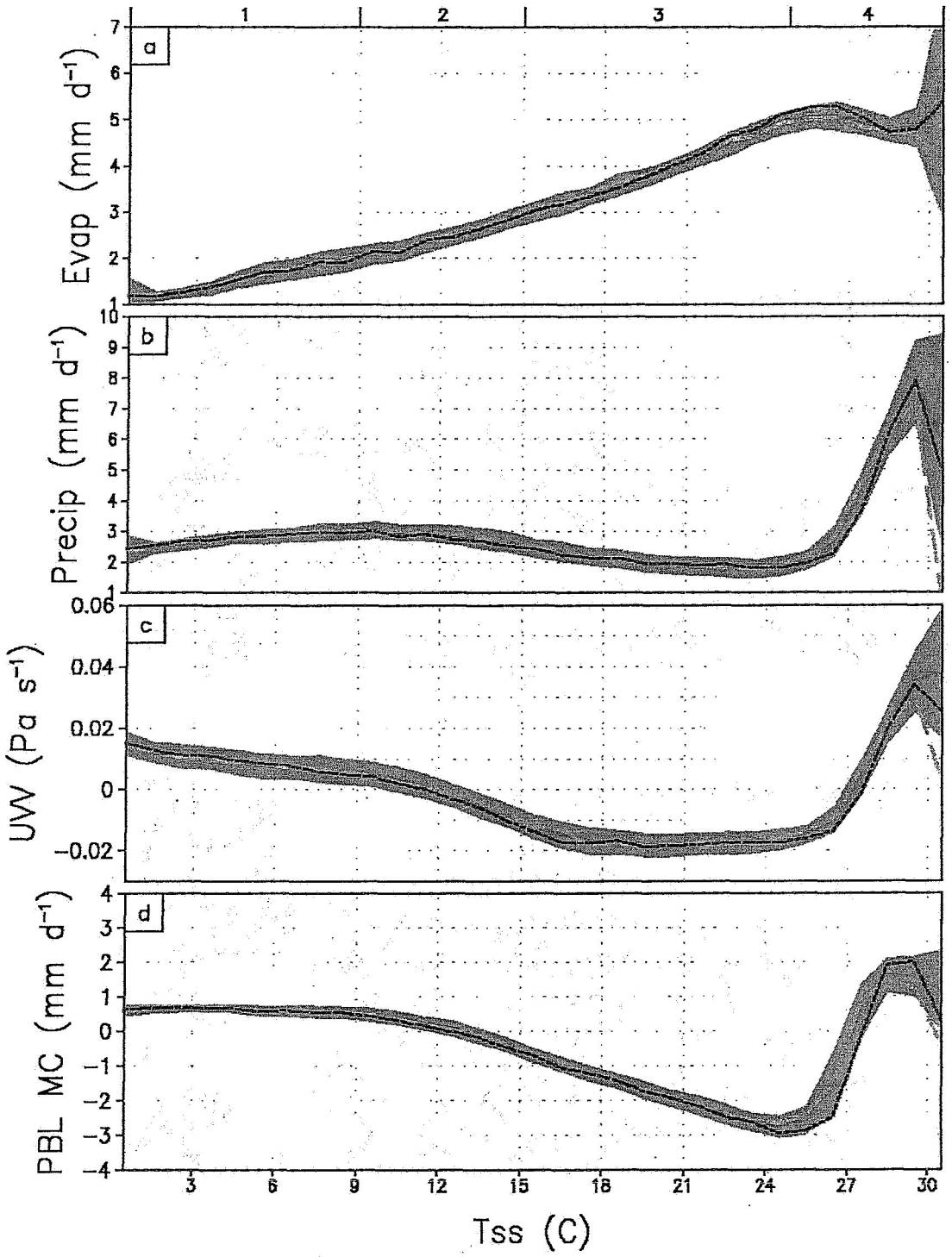

Figure 2: 120—month McRAS simulated fields of (a) evaporation, (b) precipitation, (c) 850 to 300 hPa upward vertical velocity, and (d) PBL moisture convergence, binned by Tss. Observed Tss simulation (solid green line) with standard deviation (shaded); climatological Tss simulation (long yellow dash); and 12—month 1987 El Nino Tss (short red dash).

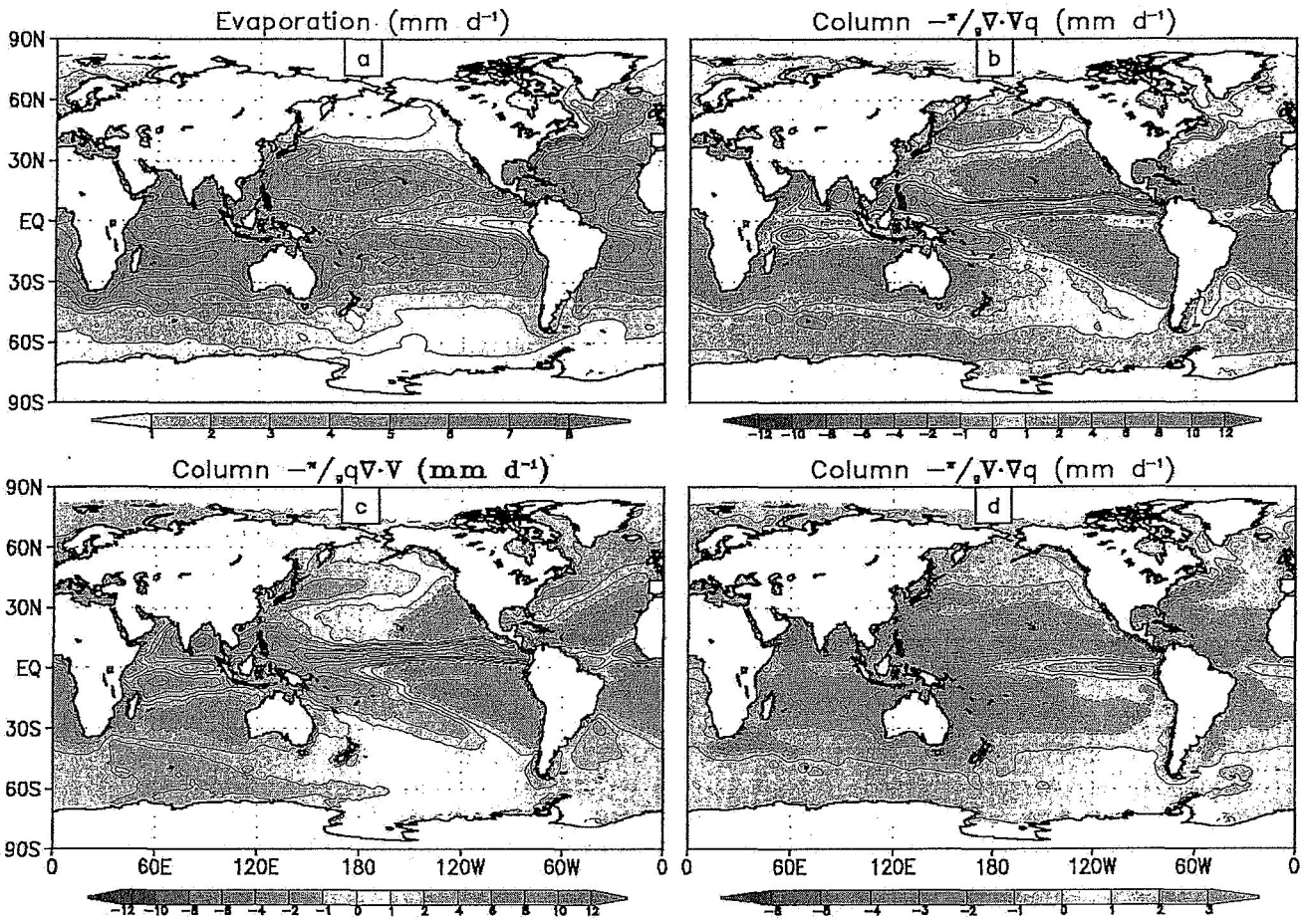

Figure 3: Evaporation and three column moisture convergence terms: a) latent heat flux, b) $-\int\nabla\cdot\nabla q$, c) $-\int q\nabla\cdot\nabla$, and d) $-\int\nabla\cdot\nabla q$ for the McRAS simulations. Contour intervals are evident in the figure.

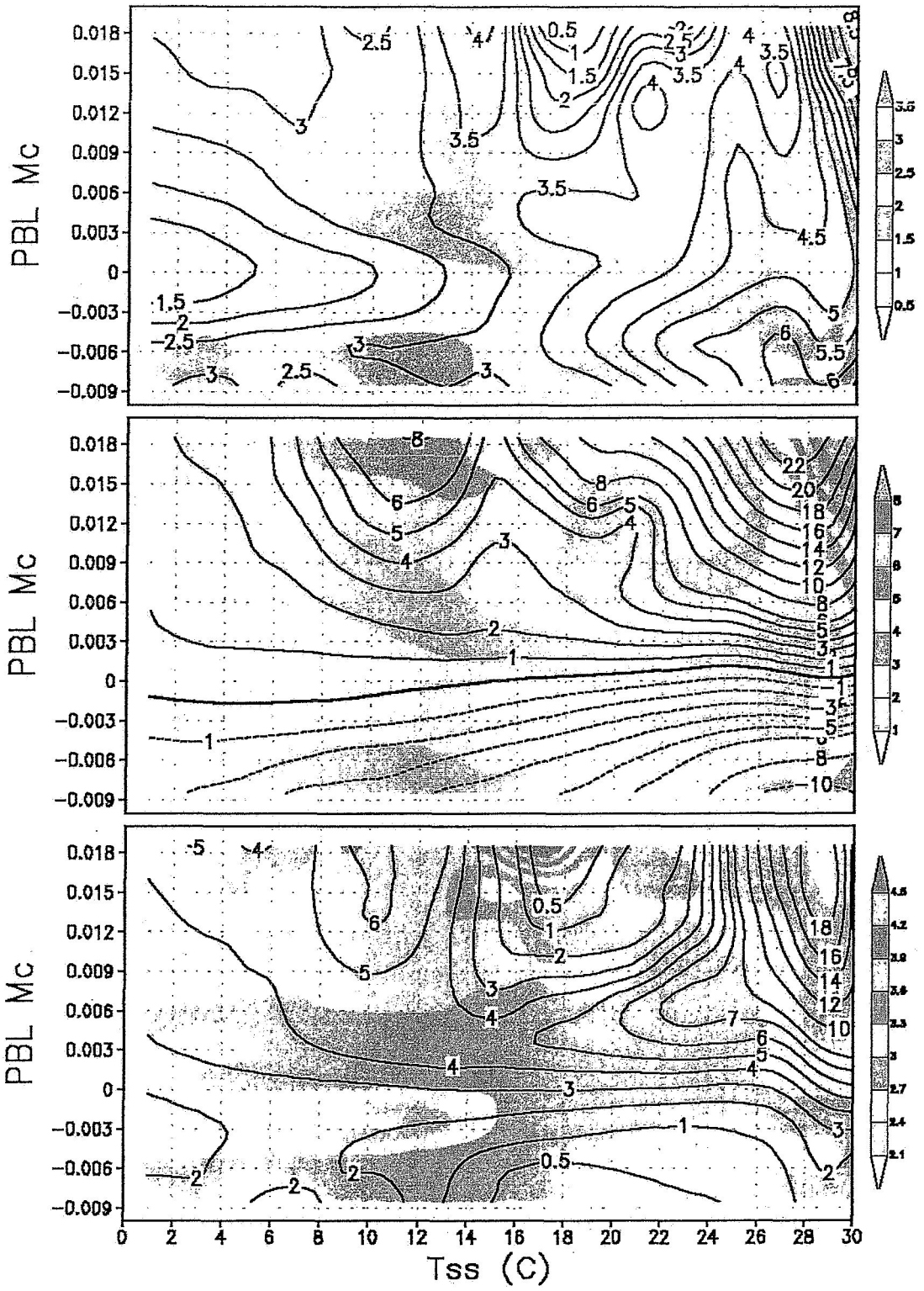

Figure 4: McRAS simulated fields, binned by Tss and PBL mass convergence (2° C Tss bins). Contours show values of a) surface latent heat flux (top), b) PBL moisture convergence (middle), and c) precipitation (bottom). Shaded values show the standard deviation of the fields for elements of each bin, except for (c), which shows the standard deviation of PBL mass convergence (kg m^{-2} hr^{-1}).

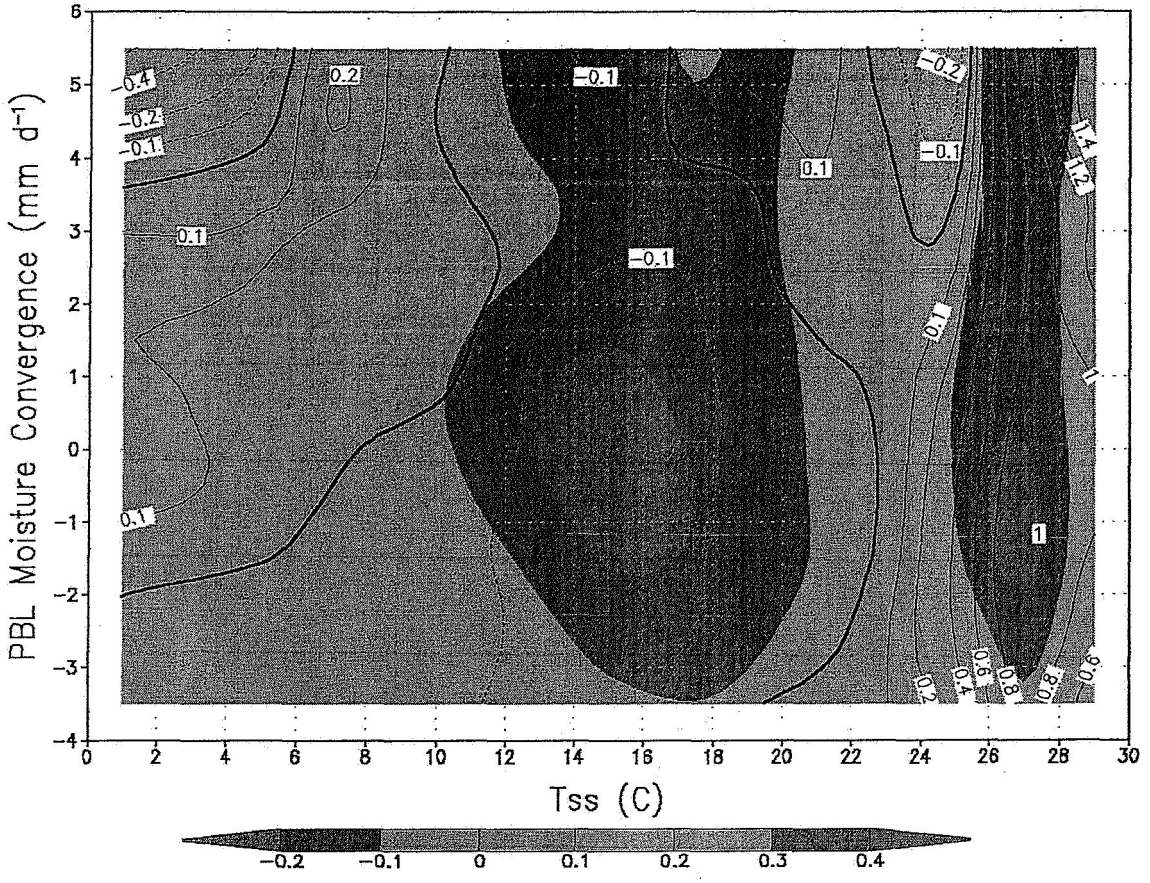

Figure 5a: McRAS simulated fields, binned by Tss and PBL moisture convergence (2°C Tss; 1 mm d^{-1} moisture convergence). Contours show values of the d(R)/d(Tss) (mm d^{-1} K^{-1}) within each bin, while the shaded background (range seen in color bar) shows $d(R)/d(MC_{PBL})*d(MC_{PBL})/d(Tss)$. Refer to section 4.5 of the text for further explanation of this figure.

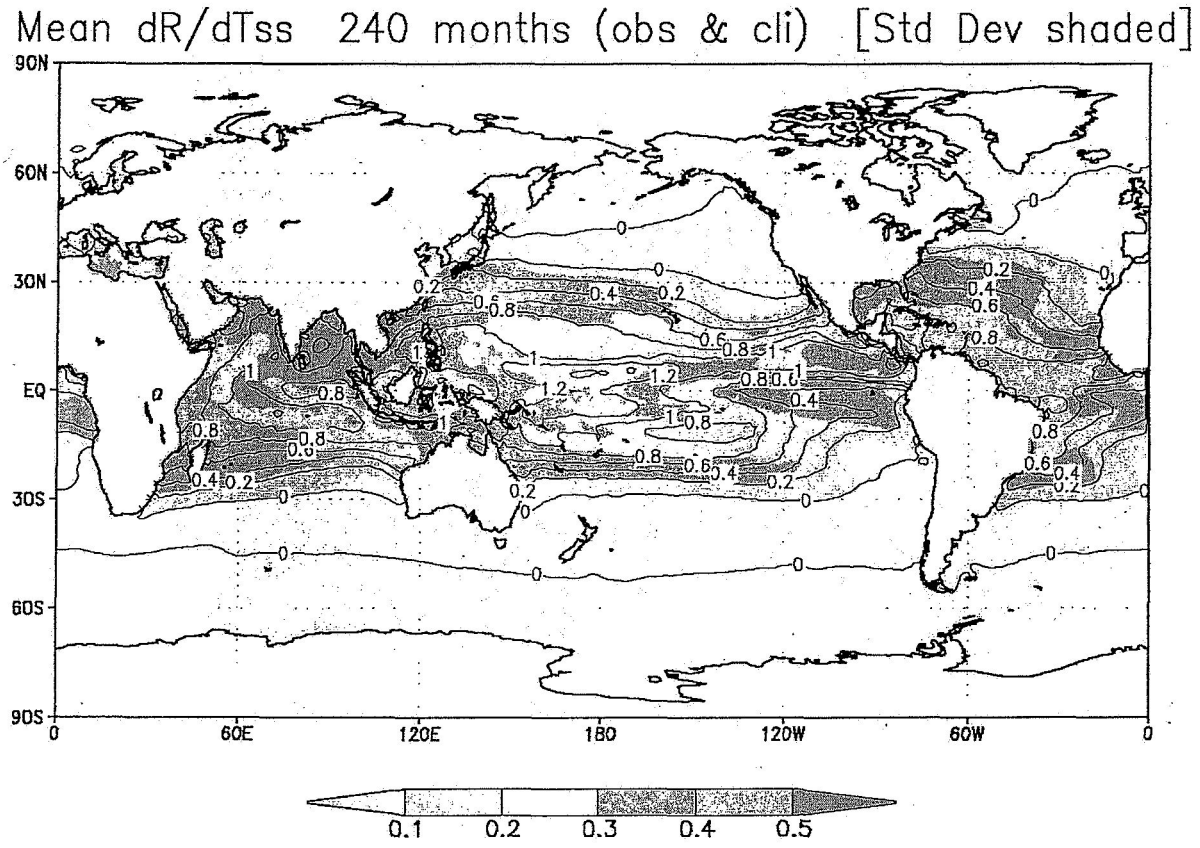

Figure 5b: Average rate of change of precipitation (mm d^{-1}) for each 1°C rise in local Tss projected from analysis in Fig. 5a. Its standard deviation for the analysis period is seen in the color shaded background.

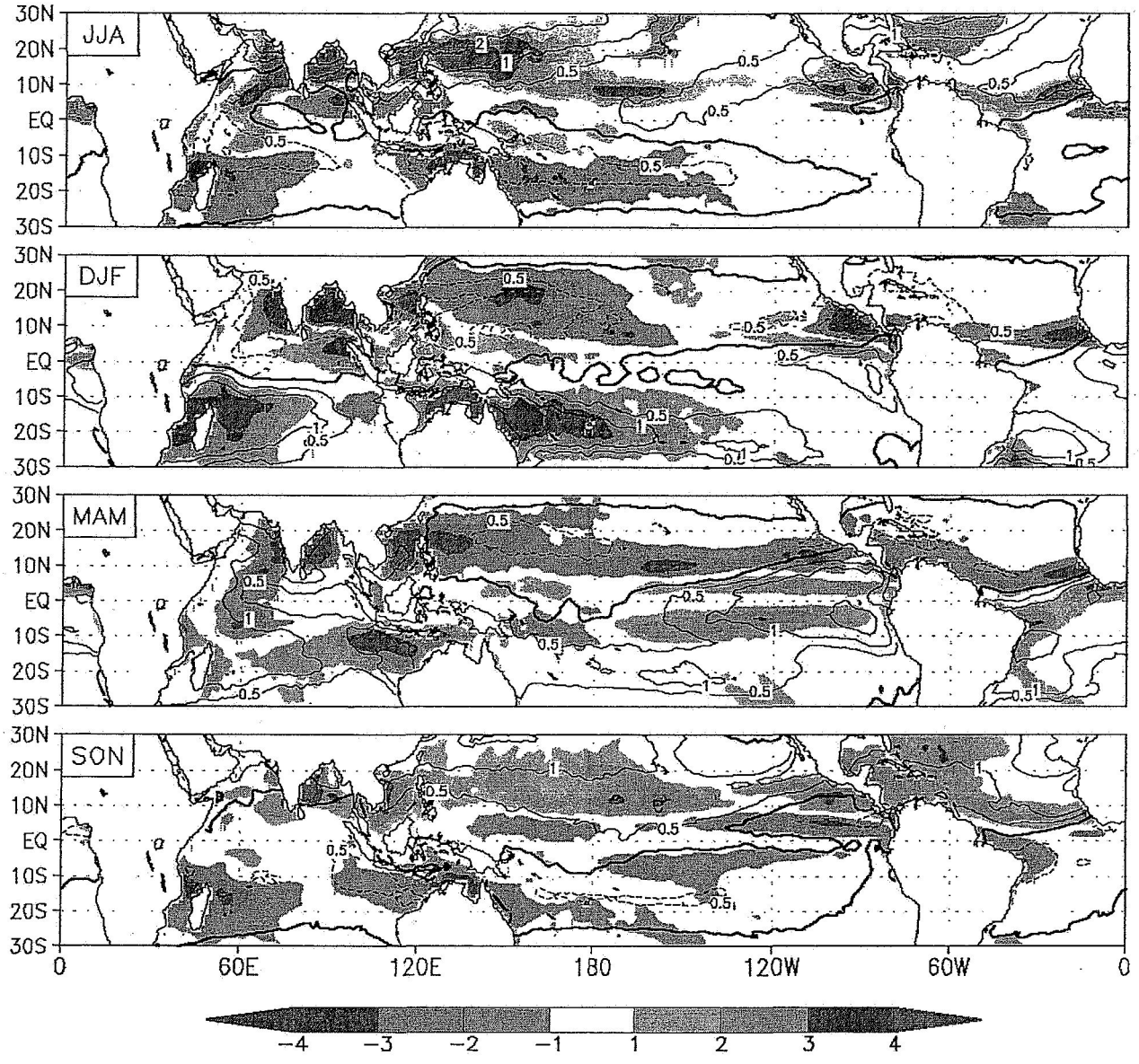

Figure 6: Four panels of seasonal changes in rainfall (mm d^{-1}) in the 10–year simulation divided into: a) influence of local Tss (contoured) and b) all effects including Tss and dynamic organization (shaded). Seasons are marked on the panels. Contours are for 0, +/− 0.5, 1, 2, 3, 4 mm d^{-1}.

Table 1: Data count in 10x15 bins.

PBL Mass Convergence ($kg\ m^{-2}\ s^{-1}$)	Tss (C) 1	3	5	7	9	11	13	15	17	19	21	23	25	27	29
0.0185	155	277	71	97	94	63	31	17	4	34	59	45	55	382	259
0.0155	330	499	168	226	264	146	101	38	37	43	52	58	132	2030	874
0.0125	908	890	422	626	705	440	295	132	72	78	113	120	315	7119	3491
0.0095	3013	1911	1390	1689	1586	1119	711	397	296	282	297	392	1078	18170	14668
0.0065	11877	6235	5144	5674	4504	3194	2307	1432	1240	1353	1456	2299	4761	50296	66643
0.0035	121087	65471	45996	37630	29348	21683	15705	11928	10594	11835	13105	17556	29324	135557	232925
0.0005	258278	249722	225161	218570	207951	177724	145458	120822	105632	97451	93148	102319	155142	318270	374645
−0.0025	16689	19683	27488	40021	56557	76749	99249	125862	153494	195574	237466	296102	360728	343430	180207
−0.0055	883	742	1021	1266	1323	1650	3829	11063	25534	26883	27148	28505	33041	36270	18955
−0.0085	109	107	185	290	257	229	590	1552	2537	2046	1465	1537	2537	3520	1684